JST: Smart Systems and Devices
Volume 35, Issue 3, September 2025, 025-033

Kalman Filter with Long Short-Term Memory for State of Charge Estimation of Lithium-Ion Battery

Nguyen Hoang Minh Giang[1], Nguyen Trong Thanh[1], Nguyen Thi Hoai Thu[1], Takano Hirotaka[2], Nguyen Duc Tuyen[1*]

[1]Power System and Renewable Energy Lab, Hanoi University of Science and Technology, Ha Noi, Vietnam
[2]Gifu University, Gifu, Japan
[*]Corresponding author email: tuyen.nguyenduc@hust.edu.vn

Abstract

The State of Charge (SOC) of the lithium-ion battery plays a vital role in monitoring and optimizing the performance of the battery management system (BMS). Traditional Kalman filter (KF) algorithm requires an accurate understanding of the dynamic model of the system and usually contains unknown statistical noises, which can make the SOC estimation inaccurate. To overcome the problem, this paper proposes a modified Kalman filter, namely Kalman-LSTM, which integrates the Long Short-Term Memory (LSTM) into the KF framework. By incorporating a neural network, the method preserves the data efficiency and interpretability of traditional algorithms while simultaneously learning the dynamic behavior of the system. The accuracy of the Kalman-LSTM method is tested using four datasets: DST, BJDST, FUDS, and US06. The SOC estimation results are then compared with different KF variants, including EKF, UKF, and AKF. The experimental results demonstrate that the proposed model has superior accuracy compared to benchmark models across various working conditions.

Keywords: State of charge, Kalman filter, neural network

1. Introduction

State of charge (SOC) is an important parameter for assessing the remaining energy in batteries and evaluating the performance of energy storage systems. However, determining SOC is a complex problem because it depends on many factors, such as battery nonlinear characteristics, environmental conditions, and charge/discharge cycles, requiring a deep understanding of the nature of batteries as well as the application of advanced models and computational methods to achieve high accuracy in SOC estimation.

To accurately estimate the SOC of a battery, it is crucial to build a suitable model. The battery model not only helps to simulate the electrochemical characteristics of the battery but also provides a theoretical basis for analyzing and predicting its performance under different operating conditions. The lithium-ion battery model can be categorized into electrochemical model [1], machine learning or data-driven model [2], and equivalent circuit model [3]. The electrochemical model provides the most detailed representation of battery behavior, enabling the simulation of underlying physical and chemical phenomena. Grounded in the principles of chemistry, physics, and fluid dynamics, this model captures key processes such as electrode reactions, ion transport within the electrolyte, and membrane interactions, providing a comprehensive framework for analyzing battery operation. The primary advantage of the electrochemical model is the ability to provide a detailed and accurate behavior of the internal mechanisms of the battery. However, a key limitation of this model is the need to solve complex partial differential equations, which demands significant computational resources and extended simulation time. Consequently, establishing and identifying the parameters of the battery model is challenging. Additionally, different battery materials necessitate distinct electrochemical models, further complicating the modeling process. Unlike electrochemical models, machine learning or data-driven models do not require an in-depth understanding of the internal mechanisms of the battery. Since these models do not rely on mathematical equations or physics-based modeling, they can rapidly learn patterns from experimental data without necessitating in-depth knowledge of the battery's structure or materials. This flexibility makes them highly adaptable and applicable across various scenarios. Given the highly nonlinear characteristics of lithium-ion battery parameters during operation, neural networks have demonstrated superior performance in capturing these complex relationships [4]. However, this approach requires a large amount of experimental data to construct effectively and validate

ISSN 2734-9373
https://doi.org/10.51316/jst.184.ssad.2025.35.3.4
Received: Feb 25, 2025; revised: Jun 24, 2025,
accepted: Jul 7, 2025

the battery model. The equivalent circuit model is used to characterize the voltage response of lithium-ion batteries during charging and discharging by representing their electrical behavior through an equivalent circuit consisting resistors, capacitors, and voltage sources. By appropriately configuring these circuit elements, the model effectively captures both the dynamic and static characteristics of the battery throughout its operating cycles [5]. Additionally, this model can be adapted to accommodate different battery types and operating conditions, making it highly versatile. Its simplicity and computational efficiency facilitate seamless integration into battery management systems (BMS) for real-time monitoring of the SOC and other key battery states.

SOC estimation methods include the Coulomb counting method [6], the open-circuit voltage (OCV)-based method [7], the impedance spectrum analysis method [8], artificial intelligence-based approaches [9], and the Kalman filter (KF) method [10]. The Coulomb counting method is widely utilized because of its simplicity and straightforward implementation, as it requires only current and time measurements, making it well-suited for systems that demand rapid computations. However, the accuracy of the KF is highly dependent on the initial SOC value and is susceptible to error accumulation over time. The OCV method based on the relationship between the OCV and the SOC of the Battery Energy Storage System (BESS). OCV provides high accuracy when the BESS is stabilized long enough before measurement and is simple to implement because it only requires voltage measurement without the need for current sensing. However, the disadvantage of the method is that the BESS needs a long time to reach equilibrium, which makes OCV ineffective in practical applications that require continuous SOC calculation. Artificial intelligence-based methods leverage deep learning techniques to model complex nonlinear relationships between SOC and various influencing factors. These approaches employ advanced algorithms such as artificial neural networks (ANN), support vector regression (SVR), and fuzzy logic to enhance estimation accuracy and adaptability [11]. These algorithms can learn from experimental data and adapt to various operating conditions without the need for precise mathematical models of the battery. However, their performance is highly dependent on the quality and volume of the training data, which directly influences the accuracy and reliability of SOC estimation. The KF is an optimal filtering algorithm widely employed for estimating the dynamic states of systems based on equivalent circuit models, particularly in nonlinear or noisy environments [12]. This algorithm requires a highly accurate battery estimation model, as well as a precise characterization of both estimation and measurement errors within the battery system. However, the stochastic nature and complexity of these errors make accurate modeling challenging. Moreover, the KF algorithm is susceptible to inaccuracies in error description, which can adversely affect estimation performance.

In real-time applications, the Extended Kalman Filter (EKF) often faces challenges in accurate modeling the measurement and process noise covariance matrices, which significantly impacts estimation performance. To address this, our work proposes a novel EKF framework where a Long Short-Term Memory (LSTM) network is trained to directly learn and infer the Kalman gain from data, bypassing the analytical computation reliant on noise covariance matrices. While prior studies have explored integrating EKF with LSTM, to the best of our knowledge, the specific formulation, training strategy, and integration of LSTM into the EKF update process presented here are unique. This approach enhances the adaptability of EKF and offers potential performance improvements in complex real-world scenarios.

Therefore, this paper proposes an extended KF enhanced with the LSTM algorithm. The LSTM is used to address model bias and the nonlinear behavior of the battery. The experimental results of the lithium-ion battery are analyzed and compared to validate the effectiveness of this method.

2. Battery Model

2.1. Second-Order RC Equivalent Circuit Model

The 2nd order RC circuit model was selected in this research because it provides a good trade-off between model complexity and accuracy for capturing the dynamic behavior of lithium-ion batteries. It includes both short-term and long-term transient responses through the use of two RC branches, which improves the representation of battery voltage relaxation compared to the 1st order model. This model has also been widely adopted in battery management literature, making it a practical and comparable choice [7, 10].

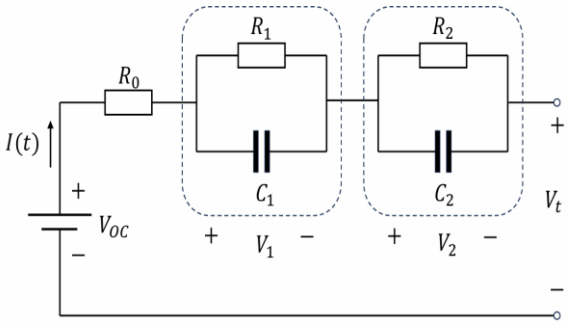

Fig. 1. Second-order RC equivalent circuit model

To estimate SOC, determining the mathematical interpretation of the battery behaviors is necessary. The second-order RC equivalent circuit model (ECM) contains an internal resistor and two RC circuits connected in series, as shown in Fig. 1. The RC circuits can simulate the characteristics caused by concentration polarization and electrochemical polarization of the battery.

According to Kirchhoff's law, the terminal voltage and the current of the ECM can be expressed as follows:

$$\begin{cases} V_{OC} = V_1 + V_2 + IR_0 + V_t \\ I = \frac{V_1}{R_1} + C_1 \frac{dU_1}{dt} \\ I = \frac{V_2}{R_2} + C_2 \frac{dU_2}{dt} \end{cases} \quad (1)$$

where V_{OC} is the open circuit voltage of the battery which is a function of SOC. V_t is the terminal voltage. I is the charging/discharging current. R_0 is the internal resistance. R_1 and C_1 are concentration polarization resistance and capacitance. R_2 and C_2 are electrochemical polarization resistance and capacitance.

The SOC of a battery is a critical parameter in battery management systems. This document presents a detailed analysis of the SOC estimation using the Ampere-hour (Ah) counting method, along with its discrete-time domain formulation and a second-order RC ECM.

According to the Ah counting method, the SOC can be expressed as:

$$SOC(t) = SOC(t_0) - \frac{\int_{t_0}^{t} I(t)\eta dt}{C_n} \quad (2)$$

where $SOC(t)$ is the SOC value of the battery at the time t. $SOC(t_0)$ denotes SOC at the initial state. η is the Coulombic efficiency. C_n represents the nominal capacity of the battery. $I(t)$ is the working current.

In the discrete time domain [13], (1) and (2) are given as follows:

$$\begin{cases} V_{t,k} = V_{OC,k} - V_{1,k} - V_{2,k} - IR_0 \\ V_{1,k} = V_{1,0} e^{\frac{-\Delta t}{\tau_1}} + IR_1 \left(1 - e^{\frac{-\Delta t}{\tau_1}}\right) \\ V_{2,k} = V_{2,0} e^{\frac{-\Delta t}{\tau_2}} + IR_2 \left(1 - e^{\frac{-\Delta t}{\tau_2}}\right) \end{cases} \quad (3)$$

where Δt is the sampling interval, τ_1=R_1C_1, τ_2=R_2C_2 are time constants.

The SOC in discrete form is:

$$SOC_k = SOC_{k-1} - \frac{\eta \Delta t}{C_n} . I_{k-1} \quad (4)$$

where Δt is the sample interval. $\tau_i = R_i C_i$ denotes the time constant.

From (3) and (4), the state space equation of the battery with a second-order RC ECM can be obtained as follows:

$$\begin{cases} x_{k+1} = F.x_k + B.u_k \\ y_{k+1} = H.x_k + D.u_k \end{cases} \quad (5)$$

where $x_k = [SOC_k \quad V_{1,k} \quad V_{2,k}]^T$ is the state variable. $u_k = I_k$ is the external input of the system. $y_k = V_{t,k}$ is the output voltage. $F, B, H,$ and D are matrix parameters which can be expressed as:

$$F = \begin{bmatrix} 1 & 0 & 0 \\ 0 & e^{\frac{-\Delta t}{\tau_1}} & 0 \\ 0 & 0 & e^{\frac{-\Delta t}{\tau_2}} \end{bmatrix} \quad (6)$$

$$B = \begin{bmatrix} -\frac{\eta \Delta t}{C_n} \\ R_1 \left(1 - e^{\frac{-\Delta t}{\tau_1}}\right) \\ R_2 \left(1 - e^{\frac{-\Delta t}{\tau_2}}\right) \end{bmatrix} \quad (7)$$

$$H = \begin{bmatrix} \frac{\partial V_{OC}[SOC_k]}{\partial SOC_k} & -1 & -1 \end{bmatrix} \quad (8)$$

$$D = -R_0 \quad (9)$$

2.2. Parameters Identification

In order to estimate SOC, it is necessary to identify the parameters in the second-order RC ECM of the battery, including R_0, R_1, R_2, C_1 and C_2. A pulse of voltage and current discharge are shown in Fig. 2.

When $t < t_0$, the battery is in steady state due to a long rest period, the input current is 0, the battery voltage is constant and equal to the open circuit voltage OCV.

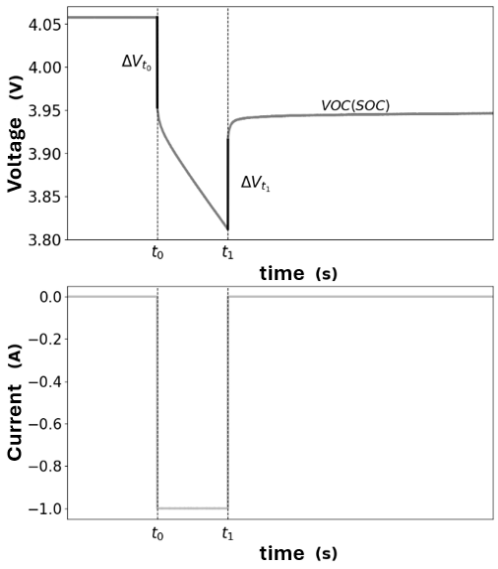

Fig. 2. Voltage and current pulse discharge used for parameter identification of the second-order RC ECM

When $t = t_0$, the sudden discharge current causes the battery voltage, which is in equilibrium and equal to OCV, to change by ΔV_1. This happens due to the internal resistance R_0.

When $t_0 < t < t_1$, with a constant discharge current, the voltage gradually decreases. At this moment, both RC circuits have current flowing through them, and the capacitor C_1 and C_2 are in the process of charging.

When $t = t_1$, as the battery stops discharging, its voltage immediately increases by ΔV_2 due to the influence of R_0.

When $t > t_1$, the battery returns to its resting state. The two capacitors, C_1 and C_2, which remain charged, begin discharging through their corresponding resistors, R_1 and R_2. This process alters the battery voltage, gradually increasing it toward the OCV.

Therefore, these parameters are determined based on the relationship between the OCV and SOC. When the battery is discharging with constant current, according to (1) and (3), the terminal voltage can be expressed as:

$$V_t(t) = V_{OC} - IR_0 - IR_1\left(1 - e^{\frac{-t}{\tau_1}}\right) - IR_2\left(1 - e^{\frac{-t}{\tau_2}}\right) \quad (10)$$

When the current varies, the instantaneous terminal voltage from $V_t(t^-)$ to $V_t(t^+)$ changes mainly by the voltage drop ΔV on the internal resistance R_0. Therefore, R_0 can be calculated by:

$$R_0 = \frac{\Delta V_1 + \Delta V_2}{2I} \quad (11)$$

Equation (10) can be rewritten by:

$$V_t(t) = V_{OC} - IR_0 - a_1\left(1 - e^{\frac{-t}{\tau_1}}\right) - a_2\left(1 - e^{\frac{-t}{\tau_2}}\right) \quad (12)$$

where the parameters of the battery model are calculated as:

$$R_1 = \frac{a_1}{I} \quad (13)$$

$$R_2 = \frac{a_2}{I} \quad (14)$$

$$C_1 = \frac{I\tau_1}{a_1} \quad (15)$$

$$C_2 = \frac{I\tau_2}{a_2} \quad (16)$$

Equations (12) to (16) will be fitted into the least squares method [14] to identify the destiny parameters for the second-order RC equivalent circuit model.

3. Kalman-Long Short-Term Memory Method for State of Charge Estimation

3.1. The Extended Kalman Filter Algorithm

The EKF [15] is a widely used algorithm in estimating the state of dynamic systems which adopts first-order Taylor expansion to linearize the nonlinear state space model as:

$$\begin{cases} x_k = f(x_{k-1}, u_{k-1}) + w_{k-1} \\ y_k = h(x_k) + v_k \end{cases} \quad (17)$$

where $f(\cdot)$ and $h(\cdot)$ are nonlinear functions. w_k and v_k are the process noise and measurement noise with Gaussian distribution Q_k and R_k, respectively.

The nonlinear functions $f(\cdot)$ and $h(\cdot)$ are linearized as in (6) and (8) with $F_k = \frac{\partial f}{\partial x_k}$ and $H_k = \frac{\partial h}{\partial x_k}$.

The EKF operates in two main phases: prediction and update.

In the prediction step, the filter estimates the current **a priori** state based on the **a posteriori** state from the previous step:

$$x_{k|k-1} = Fx_{k-1|k-1} + Bu_k + w_k \quad (18)$$

$$P_{k|k-1} = FP_{k-1|k-1}F^T + Q_k \quad (19)$$

$$y_{k|k-1} = Hx_{k|k-1} \quad (20)$$

During the update step, the filter improves the predicted state estimate by incorporating new measurements:

$$\Delta y_k = y_k - y_{k|k-1} \quad (21)$$

$$S_k = H_k P_{k|k-1} H_k^T + R_k \quad (22)$$

$$K_k = P_{k|k} H_k^T S_k^{-1} \quad (23)$$

$$x_{k|k} = x_{k|k-1} + K_k \Delta y_k \quad (24)$$

$$P_{k|k} = P_{k|k-1} - K_k H_k P_{k|k-1} \quad (25)$$

The EKF algorithm is shown in Fig. 3.

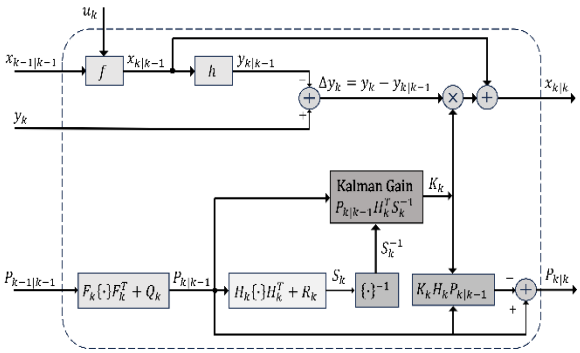

Fig. 3. EKF algorithm

In these formulations, $x_{k|k-1}$ represents the predicted (a priori) state estimate. $P_{k|k-1}$ is the predicted (a priori) estimate covariance. K_k denotes the Kalman gain. Δy_k is the innovation and S_k is the innovation covariance. $x_{k|k}$ and $P_{k|k}$ are the updated (a posteriori) state estimate and updated (a posteriori) estimate covariance, respectively.

3.2. Long Short-Term Memory

LSTM is a type of recurrent neural network used to learn the time-dependence information proposed by Hochreiter and Schmidhuber [16]. The internal memory unit and gate mechanism in the LSTM cell overcome the gradient descent of the traditional RNN. The formula of the LSTM model is shown as follows:

$$f_t = \sigma(w_f \cdot [h_{t-1}, x_t] + b_f) \quad (26)$$

$$i_t = \sigma(w_i \cdot [h_{t-1}, x_t] + b_i) \quad (27)$$

$$g_t = tanh(w_g \cdot [h_{t-1}, x_t] + b_g) \quad (28)$$

$$c_t = f_t * c_{t-1} + i_t * g_t \quad (29)$$

$$o_t = \sigma(w_o \cdot [h_{t-1}, x_t] + b_o) \quad (30)$$

$$h_t = o_t * tanh(c_t) \quad (31)$$

where f_t, i_t, g_t, and o_t are the forget gate, input gate, update gate, and output gate of the LSTM, respectively. x_t is the input data at time step t. c_t and h_t represent the cell state and hidden state, respectively. σ and $tanh$ are activation function. w_f, w_i, w_g and w_o are the weight matrices of each gate. b_f, b_i, b_g, and b_o are bias vector of the corresponding gate.

Fig. 4. Illustrates the algorithm of LSTM.

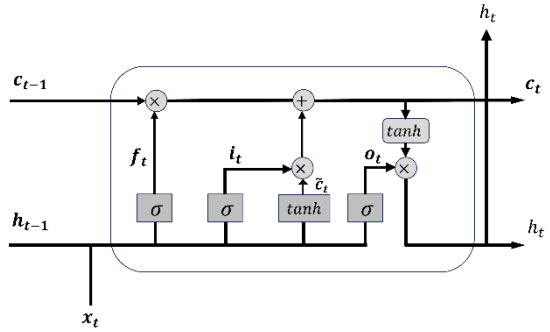

Fig. 4. LSTM memory algorithm

3.3. The Kalman-LSTM Algorithm

The core problem of the EKF is to build a model that describes the underlying dynamics based on the understanding of the system. If the parameters are inaccurate, it can affect the SOC calculation results. In this paper, we assume that the covariance matrices Q and R are unknown. These two parameters are only used during the Kalman gain calculation as shown in Fig. 3. Thus, this paper proposes a modified EKF where the LSTM will be utilized to learn the Kalman gain from the data, and alternate the Kalman gain calculation process in the EKF flow. The architecture of Kalman-LSTM is shown in Fig. 5.

A prior estimate of the current state $x_{k|k-1}$ and current observation $y_{k|k-1}$ are calculated from the previous a posteriori estimate state $x_{k-1|k-1}$ through (17). The innovation Δy_k is computed between the new observation y_k and a prior estimate of the current observation $y_{k|k-1}$.

Then, $x_{k|k-1}$ and Δy_k are concatenated to serve as input to the LSTM to output the Kalman gain. The current posterior state $x_{k|k}$ is computed by:

$$x_{k|k} = x_{k|k-1} + K_k . \Delta y_k \quad (32)$$

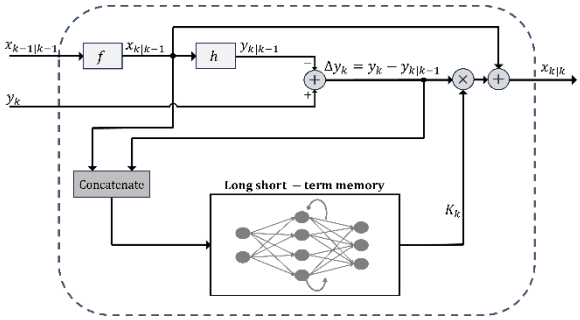

Fig. 5. Kalman-LSTM algorithm

4. Results and Discussion

4.1. Data Description

To verify the accuracy of the SOC estimation, this paper used the INR 18650-20R battery data published by the CALCE battery group [17]. Five types of experiment datasets are used, including the incremental OCV test, Dynamic Stress Test (DST), Beijing Dynamic Stress Test (BJDST), Federal Urban Driving Schedule (FUDS), and US06 Highway Driving Schedule.

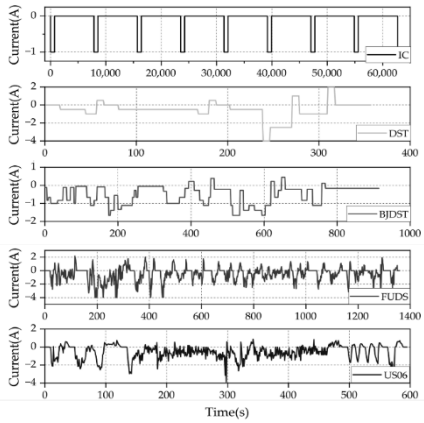

Fig. 6. Input currents in each experiment in one cycle

4.2. Benchmark Model

The benchmark models used in this study include popular state estimation algorithms such as the EKF, Adaptive Kalman Filter, and Unscented Kalman Filter. These algorithms serve as a basis for comparing and

evaluating the improvements of the proposed model. These models use $x_0 = [0.9 \quad 0 \quad 0]^T$ as the initial state, the process noice covariance and the observation measurement noise covariance are:

$$Q = \begin{bmatrix} 5 \times 10^{-6} & 0 & 0 \\ 0 & 5 \times 10^{-6} & 0 \\ 0 & 0 & 5 \times 10^{-6} \end{bmatrix}$$

and,

$$R = 0.001.$$

4.3. Model Parameter Identification

To verify the accuracy of the proposed SOC estimation method, this study utilizes battery data collected from an INR 18650-20R lithium-ion cell, which was published by the CALCE Battery Research Group at the University of Maryland [17]. Five experimental datasets are employed in the evaluation process: the Incremental Open Circuit Voltage Test, the DST, the BJDT, the FUDS, and the US06 Highway Driving Schedule. These datasets collectively represent a wide range of dynamic loading conditions, allowing for a comprehensive assessment of the model's performance under real-world scenarios.

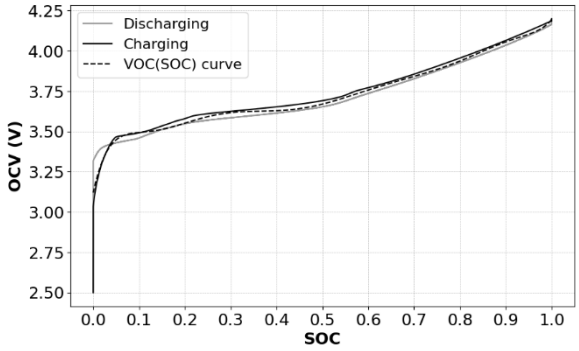

Fig. 7. SOC error under DST condition

Through the relationship curve between OCV and SOC during charging and discharging from low current OCV test as shown in Fig. 7, a ninth-order OCV-SOC curve is obtained under the constant current discharge data as:

$$\begin{aligned} V_{OC}(SOC) = {} & 1221.2SOC^9 - 5855.5SOC^8 \\ & +11841.3SOC^7 - 13093.5SOC^6 \\ & +8617.5SOC^5 - 3422.2SOC^4 \\ & +811.1SOC^3 - 108.3SOC^2 \\ & +8.072SOC + 3.228 \end{aligned} \tag{33}$$

The identification results of the second-order RC ECM parameters corresponding to each SOC value are shown in Fig. 8. The concentration polarization resistance (R_1) exhibits a non-linear variation with the SOC, reaching peak values at intermediate SOC levels and declining at both low and high SOC regions. In contrast, the electrochemical polarization resistance (R_2) demonstrates a generally increasing trend as SOC increases. The corresponding capacitances display inverse behaviors relative to their associated resistances. Specifically, the concentration polarization capacitance (C_1) decreases when R_1 increases, and the electrochemical polarization capacitance (C_2) decreases as R_2 rises. These inverse relationships reflect the dynamic electrochemical processes occurring within the battery during different stages of charging and discharging.

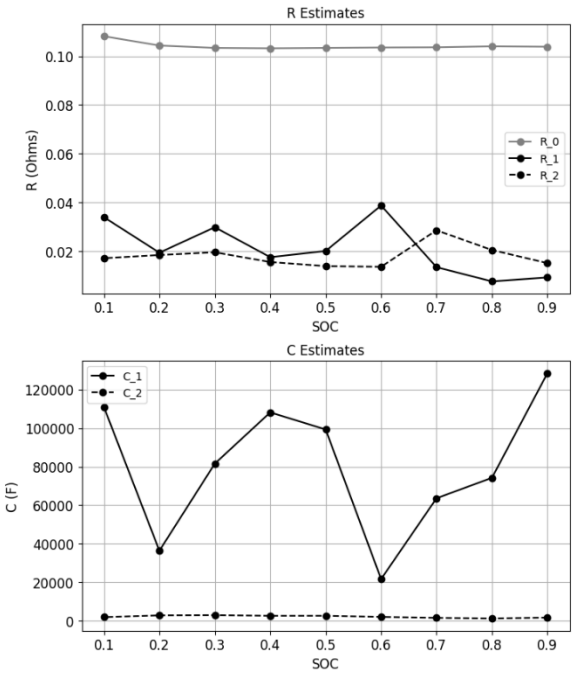

Fig. 8. Model parameters identification results corresponding to each SOC value

During the charging and discharging process, the resistance and capacitance values do not remain constant but vary within a certain range. To simplify the calculations and reduce model complexity, this paper takes the average of the calculated resistance and capacitance values as a parameter representing the battery's characteristics. The calculation results are shown in Table 1.

Table 1. Model parameters identification results

$R_0(\Omega)$	$R_1(\Omega)$	$R_2(\Omega)$	$C_1(F)$	$C_2(F)$
0.1042	0.0211	0.018	80.482.391	2.220.681

The key hyperparameters used in training the LSTM network are summarized in Table. 2. These parameters were selected based on preliminary experiments and common practices in time series modeling to ensure a balance between model

complexity and training stability. The settings include the input size, hidden layer size, number of stacked LSTM layers, dropout rate, batch size, sequence length, learning rate, optimization algorithm, and the number of training epochs.

Table 2. LSTM network configuration and training settings

Hyperparameter	Value
Input size	10
Hidden size	64
Number of layers	2
Dropout rate	0.2
Batch size	32
Training Algorithm	Adam optimizer
Learning rate	0.001
Tool	PyTorch
Training Set	70%
Validation Set	15%
Test Set	15%

4.4. State of Charge Estimation Results

The SOC estimation errors for each dataset are shown in Fig. 5. As can be seen, for the conventional Kalman algorithm, the accuracy in estimating the SOC decreases as the battery SOC approaches a low level. Specifically, when the SOC drops below the 20% threshold, the calculation error increases significantly. This phenomenon can be explained by two following primary factors:

1) The electrochemical properties of the battery change significantly when the SOC drops below 20%. At this time, the chemical reactions inside the battery gradually become less stable, reducing the accuracy of the simulation model. The model parameters, such as resistance and capacitance R_1, R_2, C_1, C_2 and available capacity, may change non-linearly when the SOC is low, increasing the complexity of accurately predicting the state of the battery.

2) Kalman algorithms often rely on cumulative calculations of previous states, where minor errors in the initial calculation steps can be amplified over multiple calculation cycles. This issue becomes particularly severe at low SOC levels, as measured signals from the system (such as voltage and current) become less sensitive and more susceptible to noise, making it more difficult for the algorithm to correct for errors.

The above problems have been effectively solved through the proposed Kalman-LSTM model when the traditional Kalman Gain calculation part is replaced by the LSTM artificial neural network. Integrating LSTM into the Kalman algorithm not only overcomes the inherent limitations of the conventional Kalman method but also brings many outstanding benefits in estimating the SOC of the battery. Specifically, the LSTM network can process and memorize information about long-term data series, making it particularly effective in identifying nonlinear and complex relationships in the data, such as the changing characteristics of the battery when the SOC is low. This allows the Kalman-LSTM model to learn nonlinear battery behaviors that conventional Kalman algorithms cannot accurately simulate. In particular, when the SOC drops below the 20% threshold, the LSTM can learn abnormal battery characteristics, such as a rapid increase in internal resistance or a significant decrease in current delivery, thereby significantly improving the model accuracy.

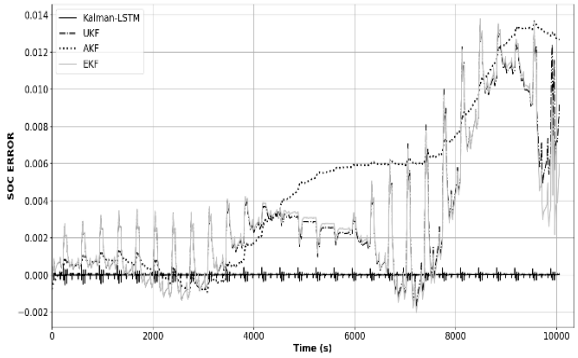

Fig. 9. SOC error under DST condition

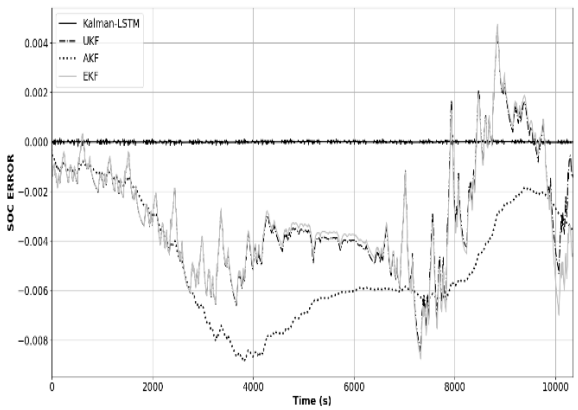

Fig. 10. SOC error under BJDST condition

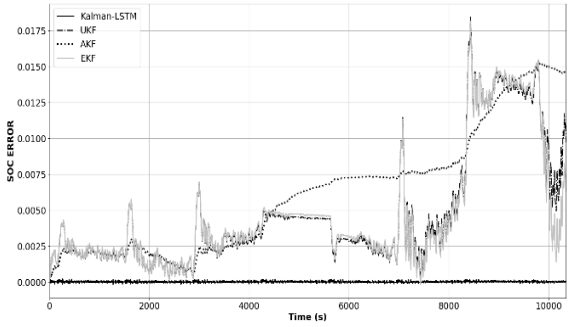

Fig. 11. SOC error under FUDS condition

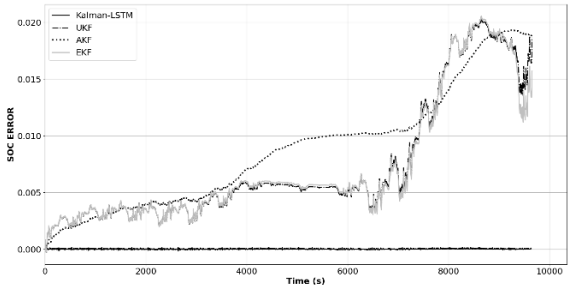

Fig. 12. SOC error under US06 condition

As can be seen from the figures, the error indices corresponding to the US06 dataset consistently have the highest values, followed by FUDS, DST, and finally BJDST. This pattern is not random but rather reflects the characteristics of the input data series, specifically the degree of battery current fluctuation. The US06 dataset represents a harsh test scenario designed to simulate real-world operating conditions with large current variations, including rapid changes in flow rate and load. Under these conditions, algorithms struggle to accurately track the SOC due to the strong nonlinearity of the battery. Sudden current changes can significantly amplify errors in the computational model over estimation cycles, leading to the largest observed error values.The FUDS dataset, while exhibiting lower current fluctuations than US06, still represents complex operating conditions with multiple alternating load phases. As a result, it also produces significant errors, though to a lesser extent than US06. In contrast, the DST dataset experiences moderate current fluctuations with more stable duty cycles, leading to lower errors compared to both FUDS and US06.

Although the BJDST dataset has a higher current oscillation frequency than DST - meaning the current changes more rapidly and frequently - the oscillation amplitude is significantly smaller. In other words, the magnitude of current change per oscillation cycle in BJDST is not as large as in DST. As a result, the impact of these fluctuations on battery SOC estimation is minimized, leading to a smaller SOC prediction error compared to DST.

A high oscillation frequency, as seen in BJDST, typically requires the model to respond quickly and efficiently to continuous current variations. However, when the oscillation amplitude is small, these variations are not large enough to cause significant shifts in key electrochemical parameters such as voltage and internal resistance. Consequently, the algorithm can maintain stability in SOC monitoring and estimation.

In contrast, DST has a lower oscillation frequency but a significantly larger amplitude. This results in greater current variations between cycles, making it more challenging to model the battery's nonlinear responses. Large current changes cause substantial variations in observed parameters, increasing the estimation errors in the algorithm.

5. Conclusion

This paper investigates and proposes a method for simulating and estimating the SOC of batteries by integrating the KF with an artificial neural network. By combining these two approaches, the proposed method demonstrates strong accuracy and effectiveness in quantifying SOC under various operating conditions. The findings demonstrate that the application of the KF effectively captures data variations while mitigating the impact of random dynamic and measurement errors. Simultaneously, the artificial neural network enhances performance by extracting complex nonlinear features, thereby significantly improving overall estimation accuracy. Furthermore, the proposed model was evaluated using real-world data collected from lithium-ion batteries. Experimental results indicate that the system not only satisfies accuracy requirements but also exhibits strong adaptability across diverse operating environments.

References

[1] W. Hao and J. Xie, Reducing diffusion-induced stress of bilayer electrode system by introducing pre-strain in lithium-ion battery, Journal of Electrochemical Energy Conversion and Storage, vol. 18, no. 2, Jan. 2021, Art. no. 020909. https://doi.org/10.1115/1.4049238

[2] S. Wang, Y. Fan, S. Jin, P. Takyi-Aninakwa, and C. Fernandez, Improved anti-noise adaptive long short-term memory neural network modeling for the robust remaining useful life prediction of lithium-ion batteries, Reliability Engineering and System Safety, vol. 230, Feb. 2023, Art. no. 108920. https://doi.org/10.1016/j.ress.2022.108920

[3] M.-K. Tran, M. Mathew, S. Janhunen, S. Panchal, K. Raahemifar, R. Fraser, and M. Fowler, A comprehensive equivalent circuit model for lithium-ion batteries, incorporating the effects of state of health, state of charge, and temperature on model parameters, Journal of Energy Storage, vol. 43, Nov. 2021, Art. no. 103252. https://doi.org/10.1016/j.est.2021.103252

[4] K. Liu, Y. Gao, C. Zhu, K. Li, M. Fei, C. Peng, X. Zhang, and Q.-L. Han, Electrochemical modeling and parameterization towards control-oriented management of lithium-ion batteries, Control Engineering Practice, vol. 124, Jul. 2022, Art. no. 105176. https://doi.org/10.1016/j.conengprac.2022.105176

[5] Q. Wang, M. Ye, M. Wei, G. Lian, and C. Wu, Co-estimation of state of charge and capacity for lithium-ion battery based on recurrent neural network and support vector machine, Energy Reports, vol. 7, pp. 7323–7332, Nov. 2021. https://doi.org/10.1016/j.egyr.2021.10.095

[6] D. Chen, L. Xiao, W. Yan, and Y. Guo, A novel hybrid equivalent circuit model for lithium-ion battery considering nonlinear capacity effects, in 6th International Conference on Advances on Clean Energy Research ICACER 2021 Apr. 15–17, 2021, Barcelona, Spain, Energy Reports, vol. 7, Sep. 2021, pp. 320–329. https://doi.org/10.1016/j.egyr.2021.06.051

[7] Y.-M. Jeong, Y.-K. Cho, J.-H. Ahn, S.-H. Ryu, and B.-K. Lee, Enhanced coulomb counting method with adaptive soc reset time for estimating ocv, in 2014 IEEE Energy Conversion Congress and Exposition (ECCE), Sep. 14-18, 2014, Pittsburgh, PA, USA, pp. 1313–1318. https://doi.org/10.1109/ECCE.2014.6953989

[8] S. Tong, M. P. Klein, and J. W. Park, On-line optimization of battery open circuit voltage for improved state-of-charge and state-of-health estimation, Journal of Power Sources, vol. 293, pp. 416-428, Oct. 2015. https://doi.org/10.1016/j.jpowsour.2015.03.157

[9] J. A. A. Qahouq and Z. Xia, Single-perturbation-cycle online battery impedance spectrum measurement method with closed-loop control of power converter, IEEE Transactions on Industrial Electronics, vol. 64, no. 9, Sep. 2017, pp. 7019-7029. https://doi.org/10.1109/TIE.2017.2686324

[10] X. Hu, H. Yuan, C. Zou, Z. Li, and L. Zhang, Co-estimation of state of charge and state of health for lithium-ion batteries based on fractional-order calculus, IEEE transactions on vehicular technology, vol. 67, iss. 11, pp. 10319-10329, Nov. 2018. https://doi.org/10.1109/TVT.2018.2865664

[11] Vu, Nga Thi-Thuy, Nam Phuong Tran, and Nam Hoai Nguyen, Adaptive neuro-fuzzy inference system based path planning for excavator arm, Journal of Robotics, iss. 1, Dec. 2018, Art. no. 2571243. https://doi.org/10.1155/2018/2571243

[12] Nguyen, Nam H., and Martin Hagan, Stability analysis of layered digital dynamic networks using dissipativity theory, The 2011 International Joint Conference on Neural Networks, IEEE, 2011. https://doi.org/10.1109/IJCNN.2011.6033428

[13] Y. Wang and Z. Chen, A framework for state-of-charge and remaining discharge time prediction using unscented particle filter, Applied Energy, vol. 260, Feb. 2020, Art. no.114324. https://doi.org/10.1016/j.apenergy.2019.114324

[14] Plett, Gregory L. Battery Management Systems, Volume I: Battery Modeling. Artech House, 2015.

[15] F. Ding, Least squares parameter estimation and multi-innovation least squares methods for linear fitting problems from noisy data, Journal of Computational and Applied Mathematics, vol. 426, Jul. 2023, Art. no. 115107. https://doi.org/10.1016/j.cam.2023.115107

[16] L. J. Dang, Y. L. Huang, Y. G. Zhang, B. D. Chen, Multi-kernel correntropy based extended Kalman filtering for state-of-charge estimation, ISA Transactions, vol. 129, part B, pp. 271-283, Oct. 2022. https://doi.org/10.1016/j.isatra.2022.02.047

[17] Hochreiter, S., Schmidhuber, J., Long short-term memory, Neural Computation, Nov. 1997, vol. 9, pp. 1735-1780. https://doi.org/10.1162/neco.1997.9.8.1735